One-dimensional nanoclustering of the Cu(100) surface under CO gas in the mbar pressure range

Baran Eren [a,1], Danylo Zherebetskyy [a,b,1], Yibo Hao [a], Laerte L. Patera [a,c,d], Lin-Wang Wang [a], Gabor A. Somorjai [a,e], Miquel Salmeron [a,f,*]

[a] Materials Sciences Division, Lawrence Berkeley National Laboratory, 1 Cyclotron Road, Berkeley, CA 94720, United States
[b] Nanosys Inc., Milpitas, CA 95035, United States
[c] CNR-IOM, Laboratorio TASC, Strada Statale 14, Km. 163.5, I-34149 Trieste, Italy
[d] Physics Department and CENMAT, University of Trieste, via A. Valerio 2, I-34127 Trieste, Italy
[e] Department of Chemistry, University of California, Berkeley, United States
[f] Department of Materials Science and Engineering, University of California, Berkeley, United States

ARTICLE INFO

Article history:
Received 18 March 2016
Received in revised form 15 April 2016
Accepted 15 April 2016
Available online 9 May 2016

Keywords:
Cu(100)
Carbon monoxide
Nanoclustering
HPSTM
DFT

ABSTRACT

The bulk terminated Cu(100) surface becomes unstable in the presence of CO at room temperature when the pressure reaches the mbar range. Scanning tunneling microscopy images show that above 0.25 mbar the surface forms nanoclusters with CO attached to peripheral Cu atoms. At 20 mbar and above 3-atom wide one-dimensional nanoclusters parallel to <001> directions cover the surface, with CO on every Cu atom, increasing in density up to 115 mbar. Density functional theory explains the findings as a result of the detachment of Cu atoms from step edges caused by the stronger binding of CO relative to that on flat terraces.

1. Introduction

Decades of surface science studies performed in ultra-high vacuum (UHV) have established the foundation of our present understanding of solid surfaces [1–2]. These studies provided insight to many scientific and technological fields, including catalysis with semiconductor and metal surfaces [1]. In real life applications however, the surface of materials constantly interact with surrounding matter. Especially at the solid-gas interface it is of utmost importance to bridge the so-called 'pressure gap' between surface science studies in UHV and under high gas pressures, and to cover a large part of the thermodynamic phase diagram rather than a single point which is often out of equilibrium. High pressure scanning tunneling microscopy (HPSTM), the technique used here, was developed in an attempt to understand the response of the atomic structure of the solid surfaces to adsorption of molecules in equilibrium with ambient gas [3–8].

Probably the most important aspect where surface science at ambient pressures departs from its traditional counterpart is mass transfer processes involving large scale surface reconstructions driven by the weakening of the metal–metal bonds of surface atoms and maximization of the energy gained through adsorption. Recent results demonstrated this in a dramatic way. A recent example showed that although the compact (111) face of Pt remains flat and stable in the presence of up to 1 bar of CO [9], the stepped (557) and (332) surfaces reconstruct readily, adopting a completely different atomic structure from that under vacuum conditions. The second example involves Cu(111), the most compact and stable face of this metal, which decomposes into nanoclusters at CO pressures as low as 0.25 mbar [10]. Cu has a lower cohesive energy (i.e., it is softer) than Pt, which allows its surface to undergo mass transfer at lower pressure at ambient temperature. These findings open the question as to whether other soft metals (e.g. Au, Ag, Zn, etc.), or other facets of Cu behave similarly. To determine the generality of the phenomenon we extend here our study to the (100) face, the second most compact and stable surface of Cu. The choice of the CO/Cu system is fueled by its technological relevance in various catalytic reactions such as the water-gas shift, methanol synthesis and oxidation, CO_2 hydrogenation, and CO oxidation [11–20]. Here, we show that the Cu(100) surface also decomposes into nanoclusters in the presence of 0.25 mbar or higher of CO at room temperature (RT), but with a structure that is quite different from the ones observed on Cu(111). We show that the nanoclusters evolve from small ones, with a CO-adlayer of $(\sqrt{2} \times \sqrt{2})R45°$ periodicity, to elongated 3-atom wide one-dimensional clusters when the CO coverage exceeds 0.5 monolayers (ML) at gas pressures in the 100 mbar range and higher.

* Corresponding author.
E-mail address: mbsalmeron@lbl.gov (M. Salmeron).
[1] These authors have contributed equally to this work.

http://dx.doi.org/10.1016/j.susc.2016.04.016

2. Experimental

A clean Cu(100) surface was prepared by several cycles of Ar^+ sputtering (1 keV, 15 min) and annealing (793–823 K, 10 min). CO gas was introduced through a leak valve after passing through a carbonyl trap to the measurement chamber, starting at a base pressure of 1×10^{-10} mbar. The pressure was measured with MKS 722A Baratron and Convectron Pirani pressure gauges. HPSTM measurements were performed at RT in a home-built STM using Pt/Ir tips [6]. The STM was operated in constant current mode, with the bias voltage applied to the sample. Images were acquired between 15 and 60 min after gas introduction. The chemical composition of the surface was checked with Auger electron spectroscopy after each experiment. We checked in particular that no nickel contamination (from potential Ni-carbonyls) had occurred.

3. Theory

Density functional theory (DFT) calculations were performed using the VASP software package [21]. The projector augmented wave (PAW) method was utilized to construct the basis set for the one-electron wave functions, with a plane-wave basis with cutoff energy of 420 eV [22]. The Cu(100) was modeled by slabs of 5 atomic layers separated by a 22 Å of vacuum. A $7 \times 7 \times 1$ Monkhorst-Pack k-point grid was used in a $2 \times 2 \times 5$ slab to find an optimal computational approach for CO adsorption. Further calculations used an accordingly scaled k-point grid. The energy convergence was established at 10^{-5} eV, while the force convergence was set at 3×10^{-3} eV/Å.

Among the functionals applied to the $2 \times 2 \times 5$ slab, the PBE + U in the Dudarev's approach [23], with U = 7 eV for C and O atoms provides both the correct CO adsorption site on top-sites and an adsorption energy of −0.63 eV for 0.125 ML coverage (see Table 1 for benchmarking of all the tested functionals), in agreement with experiment [24]. The PBE + U functional was used for further cluster calculations.

4. Results and discussion

4.1. HPSTM images of the nanoclusters

Fig. 1a shows the HPSTM image of the Cu(100) surface in the presence of 0.25 mbar of CO. The surface appears covered with rectangular nanoclusters with edges oriented along <001> directions. The steps edge atoms of nanoclusters and terraces are spaced by $\sqrt{2}$ times the Cu-Cu distance as a result of CO adsorption. Away from the edges, several terrace regions are seen with the (1×1) periodicity characteristic of the clean surface (Fig. 1c). Fig. 1b shows examples of two small 5 atom nanoclusters, later used as model in our DFT calculations. The corners of the nanoclusters have high contrast spots, which we attribute to adsorbed CO.

Table 1
Comparative energetics of CO adsorption on bridge and hollow sites (E_{bridge} and E_{hollow}) relative to the top sites (E_{top}) on the Cu(100) surface using different exchange-correlation functionals. The surface slab dimension is 2×2 atoms wide and 5 atomic layers thick. Negative values indicate a more favorable energy for the top site. Only the PBE + U with U = 7 predicts a top configuration of CO and adsorption energy of −0.63 eV in agreement with experiment (highlighted in bold) [24].

Method	E_{top}-E_{bridge}, eV	E_{top}-E_{hollow}, eV
LDA	0.21	0.41
PW91	0.05	0.15
PBE	0.05	0.16
PBEsol_PS	0.15	0.31
revPBE-vdW(DF)	−0.01	0.08
rPW86-vdW(DF2)	−0.01	0.01
PBE + U(1)	0.05	0.15
PBE + U(4)	−0.01	0.06
PBE + U(7)	**−0.10**	**−0.18**

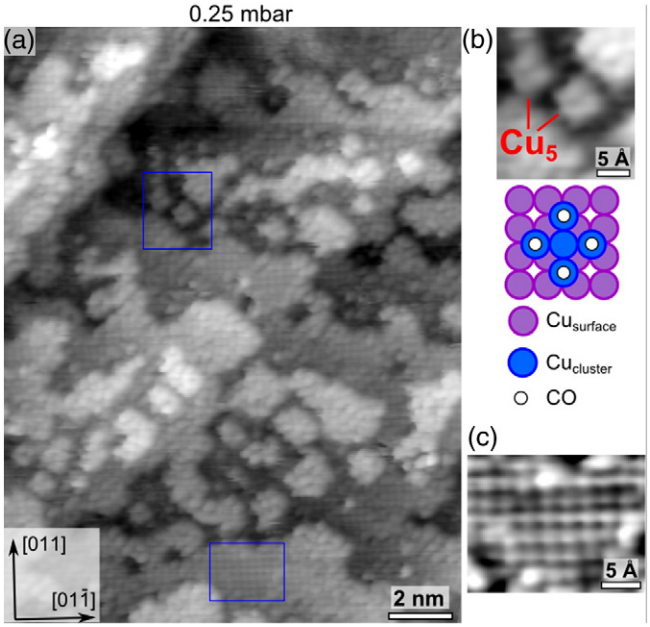

Fig. 1. (a) Cu(100) surface in the presence of 0.25 mbar of CO. The surface breaks up into nanoclusters with edges oriented in the <001> directions. Imaging parameters: [V_b = 0.5 V, I_t = 0.5 nA]. (b) Example showing 5 atom clusters from the top framed box in (a), with a proposed ball model below. (c) Expanded view of the area in the lower box in (a), exhibiting the (1×1) periodicity characteristic of clean Cu(100).

The nanoclusters increase in number and size as the CO pressure increases. Fig. 2a-i shows an HPSTM image of the surface in the presence of 20 mbar of CO. Two structures are observed. A few regions on the surface have a local $(\sqrt{2} \times \sqrt{2})R45°$ arrangement, similar to that formed at saturation coverage in UHV at cryogenic temperatures [25], with a local coverage of 0.5 ML. The second and more dominant structure consists of elongated 3-atom wide nanoclusters (Fig. 2a–ii) oriented along <001> directions. As the pressure is increased to 115 mbar (Fig. 2b–i), the elongated nanoclusters appear more numerous than at 20 mbar. Both in Fig. 2a–ii and in Fig. 2b–ii, the spots, due to CO, form a zigzag pattern along the <001> directions, with the central line of molecules showing higher contrast than those in adjacent lines. As will be justified later with DFT calculations, the zig-zag originates from CO molecules repelling each other, as previously found in UHV at high CO coverage [26]. The higher contrast of the central line is due to CO molecules pointing upwards whereas they are tilted sideways in the adjacent rows due to repulsion between neighboring molecules. Most of the one-dimensional nanoclusters in Fig. 2b–i are separated by roughly 1 nm from each other, probably dictated by steric repulsion.

4.2. Energetics of cluster formation

It is well-known that terraces contain mobile Cu adatoms detached from kink sites [27]. This is an equilibrium property of the surface at RT, with a formation energy of Cu adatoms calculated as 0.60 eV. However, CO binds stronger to the under-coordinated Cu adatoms than to the (100) terrace Cu atoms (with calculated binding energies of −0.84 eV and −0.63 eV, respectively). This stronger binding reduces the formation energy of single CuCO complexes on the (100) terrace to 0.39 eV so that they can form more easily [10,28]. The CuCO complexes can then agglomerate into small nanoclusters, such as the Cu_5 clusters shown in Fig. 1b, and others that are not well resolved in Fig. 1a, which can then aggregate to form larger and more stable nanoclusters (Table 2). We should also note that the formation of nanoclusters is a dynamic process so that the surface evolves continuously but slowly at RT on the scale of tens of minutes.

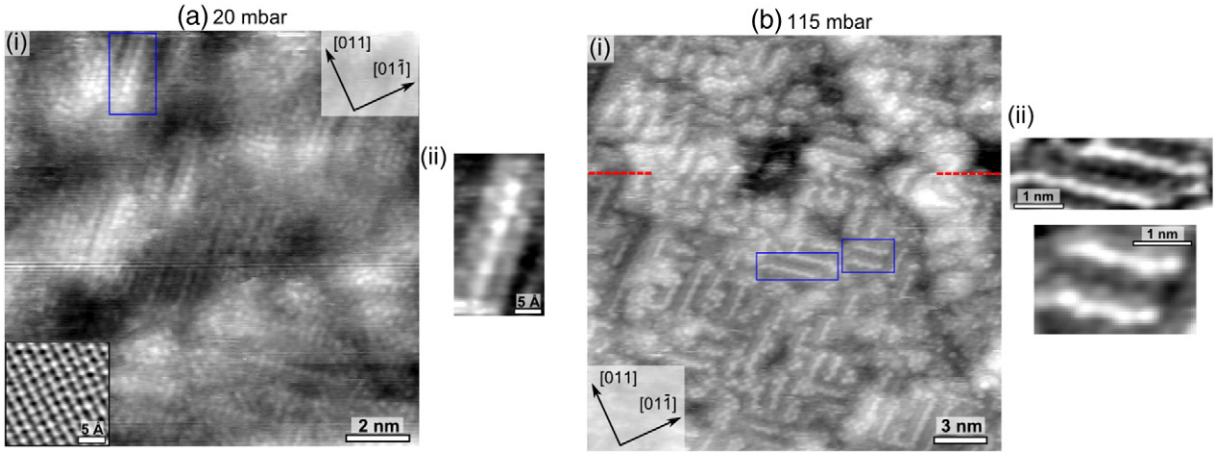

Fig. 2. Cu(100) surface in the presence of 20 mbar of CO. Imaging parameters: [$V_b = -0.03$ V, $I_t = 1.8$ nA]. The inset in the lower left shows an image of the Cu(100) surface in UHV providing the crystal orientation. Imaging parameters: [$V_b = 0.3$ V, $I_t = 3.6$ nA]. New 3-atom wide elongated structures are formed at this pressure. (a–ii) Magnified view of the linear nanoclusters in the box in (a–i). The central line of molecules shows a weak zig-zag order. (b–i) Cu(100) surface in the presence of 115 mbar of CO. Imaging parameters: [$V_b = 0.55$ V, $I_t = 1.25$ nA]. b–ii show examples of linear nanoclusters. The zig-zag structure is more apparent in the lower part of this image. The dashed red line in (b–i) indicates an abrupt change of the tip which changes the STM contrast, causing the central row to appear brighter than before and the zig-zag amplitude enhanced.

Although the PBE + U approach in DFT calculations provides experimentally verified results for the surface-molecule interaction, it lacks attractive molecular van der Waals (vdW) interactions and reproduces the coverage-dependent adsorption energies from experiments only qualitatively [24]. The vdW interaction between molecules provides up to −43.5 meV per CO of additional binding on the linear nanoclusters (in vdW-DF approach [29,30]). The formation energies were calculated as:

$$E_{Form} = E_{tot}(slab + clust + N_{CO}) - E(slab) - \Delta N_{Cu}\cdot\mu_{Cu} - N_{CO}\cdot\mu_{CO} \qquad (1)$$

Here ΔN_{Cu} is the number of Cu in the nanocluster; μ_{Cu} is calculated from the bulk Cu energy; and N_{CO} is the number of CO molecules in the cluster. We have also included van der Waals interactions among CO molecules in the total energy: $E_{tot}(slab + clust + N_{CO})$. μ_{CO} is the chemical potential of CO, either in the gas phase or on the flat Cu surface in chemical equilibrium. μ_{CO} can be calculated from $E_{CO}^{vac} + E_{CO}^{bind}$, here E_{CO}^{vac} is the total energy of a single CO in vacuum and E_{CO}^{bind} is the surface binding energy of CO on the flat surface for a given coverage. The energy per Cu atom in the cluster (calculated using a 2 × 2 × 6 slab) is −3.726 eV, slightly smaller than the bulk atomic energy of −3.96 eV. This energy is used for the estimation of the cluster formation energies in Eq. (1). We have taken the experimental value of $E_{CO}^{bind} = -0.48$ eV for a 0.5 ML coverage at 20 mbar [24].

The cluster formation energies with and without CO molecules are summarized in Table 2. The formation energy of +0.39 eV for Cu(CO) is small enough for its formation to occur at room temperature. Cu(CO) clusters can aggregate to form larger $Cu_4(CO)_4$, $Cu_5(CO)_4$ and $Cu_5(CO)_5$ clusters, and thus gaining energy (these clusters are more stable than separated Cu(CO) units). Among tested models of the linear clusters derived from the experimental images, the $[Cu_3(CO)_3]$f cluster consisting of three lines of Cu atoms with CO on top (Fig. 3f) is the most stable ($E_{form} = -90$ meV per periodic unit $[Cu_3(CO)_3]$f from Eq. (1) at coverages above 0.5 ML (Table 2). Summarizing the calculated results: 1) the initial flat surface breaks up into clusters, because of the small formation energy (0.39 eV) of CuCO complexes, which at RT can detach from the step edges and subsequently aggregate in the terraces to form small clusters and 2) larger linear nanoclusters are formed when the CO coverage/pressure is high enough to compensate for the reduced adsorption energy of CO so that the large clusters, with denser CO coverage become thermodynamically stable.

Table 2
Formation energies of various $Cu_x(CO)_y$ clusters on Cu(100) calculated using the PBE + U(7) approximation, as shown in Eq. (1) in the text. The energy gain from CO adsorption is compared to the CO adsorption energy on the (100) terrace at 0.5 ML coverage of −0.48 eV [24]. Increasing of the coverage decreases the terrace adsorption, indicating the clusters to be more stable. [cluster] denotes infinite periodic linear clusters. $[Cu_x(CO)_y]$a-f denote the infinite linear clusters shown in Fig. 3 from top to bottom. Only the $[Cu_3(CO)_3]$f cluster (Fig. 3f) is energetically favorable (highlighted in bold).

Cluster	E_{form}, eV	E_{ads}(CO), eV/mol	E_{vdW}, eV/mol
Cu	+0.60		
Cu_4	+1.21		
Cu_5	+1.68		
$[Cu_1]$	+0.56		
$[Cu_3]$	+0.58		
$[Cu_4]$	+1.19		
Cu(CO)	+0.39	−0.84	0
$Cu_4(CO)_4$	+0.18	−0.73	$-8.3\cdot10^{-3}$
$Cu_5(CO)_4$	+0.36	−0.81	$-5.0\cdot10^{-3}$
$Cu_5(CO)_5$	+0.27	−0.75	$-11.3\cdot10^{-3}$
$[Cu_{4(}CO)_3]$a	+1.48	−0.34	$-40.7\cdot10^{-3}$
$[Cu_{4(}CO)_3]$b	+0.77	−0.59	$-25.2\cdot10^{-3}$
$[Cu_{4(}CO)_4]$c	+1.38	−0.39	$-38.1\cdot10^{-3}$
$[Cu_{1(}CO)_3]$d	+0.37	−0.51	$-31.1\cdot10^{-3}$
$[Cu_{1(}CO)_3]$e	+0.42	−0.48	$-43.5\cdot10^{-3}$
$[Cu_3(CO)_3]$f	**−0.09**	**−0.67**	**$-32.2\cdot10^{-3}$**

4.3. Simulated images of the nanoclusters

A detailed look at the 3-atom wide one-dimensional nanoclusters shows that the central row is shifted one half-period along the <001> direction relative to the side rows. The contrast of this row is also higher, suggesting a different height and electronic structure compared to the side rows. We use DFT + U calculations to understand the structure of the nanoclusters, modeling them as infinite periodic linear chains. Among the various models considered (Fig. 3), nanoclusters consisting of three lines of Cu atoms with CO on top (Fig. 3f) was found to have the lowest formation energy of −90 meV per periodic unit (3 Cu + 3 CO molecules). This value might not be accurate within tens of meV due to the intrinsic error in DFT calculations as well as the uncertainty of the experimental chemical potential used in Eq. (1). Nevertheless, the relative order of the formation energies among different clusters should be reliably predicted by DFT. The side CO molecules fan out by 33° due to CO-CO repulsion, increasing the width of the nanoclusters to 7.38 Å, in agreement with the observed ~7.5 Å in Fig. 2a–ii and b–ii.

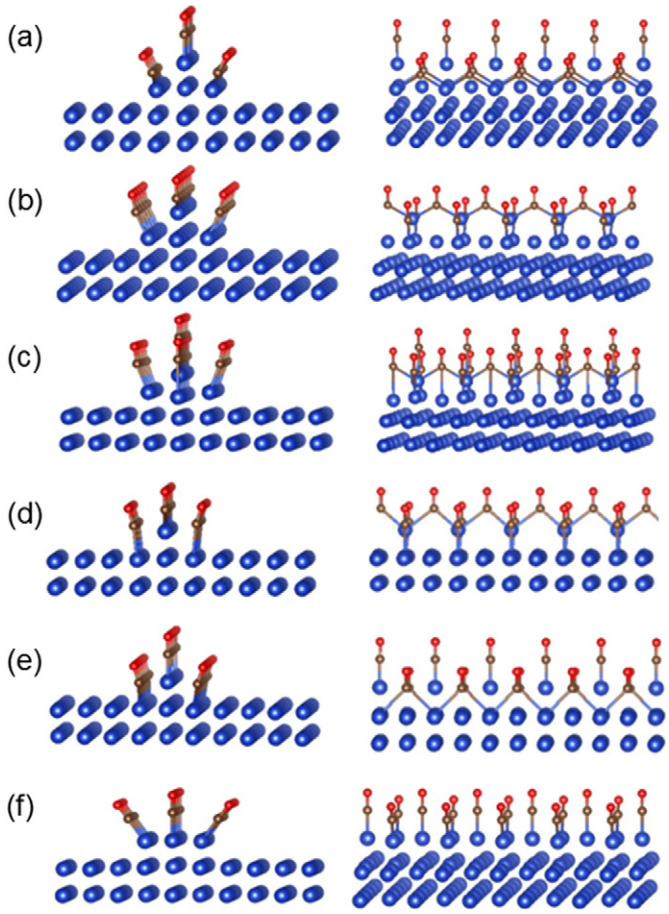

Fig. 3. Side views of various atomic structures that can possible generate the observed STM images. In (a–c) clusters are modeled with 4 Cu rows (1 on top and 3 underneath), in (d–e) the clusters are modeled as a single Cu row, and in (f) the cluster is modeled as 3 Cu rows with different CO conformations on the surface. Number of CO molecules per Cu atom is indicated in Table 2. In (a–e), the periodicity observed experimentally is obtained by alternatively placing CO molecules to top and bridge sites, whereas in (f) all CO molecules occupy the top sites. The energetic stability of these clusters, calculated with the DFT + U approach, is shown in Table 2. Only the $[Cu_3(CO)_3]$f shown in (f) is found to be energetically favorable.

The molecules of the central row exhibit also a slight zig-zag angle of 3°, due to CO–CO repulsion. Since the CO molecules in the central row remain almost normal to the surface while the side molecules fan out, they appear higher than the side molecules by 0.68 Å. This explains their higher brighter in the experimental STM images. STM images for the most stable DFT structures were also calculated within the Tersoff-Hamann approach, where the tunneling current is proportional to the sum of local charge densities evaluated at the tip (r_t) over the energy range E_F to $E_F + V$ [31].

The tunneling probability was approximated by:

$$T(\mathrm{E}) \sim \exp(-z\sqrt{\frac{8m_e}{\hbar^2}(\mathrm{V}-\mathrm{E})}, \quad (2)$$

where z is the tip-sample distance, V is the tunneling barrier height, E is the energy of tunneling electrons.

We simulated STM images with different periodicities between linear clusters. Examples of simulations of the three atom wide linear clusters with periodicities of 4, 5 and 7 atoms as shown in Fig. 4a, b, and c, respectively. The simulated image in Fig. 4b, visualized using the Hive package [32], shows a lateral periodicity between parallel clusters of 10.8 Å, which is equivalent to 2 missing rows between clusters. This is close to the ~1 nm periodicity observed in the experimental images (e.g. Fig. 2b–ii). In the experimental images, the zig-zag and contrast of the central row vary in different images, even when same imaging parameters are used at the same CO pressure. We believe that this is due to differences in the tip structure at ambient pressures. For instance, the horizontal dashed lines in Fig. 2b–i indicate a tip change which results in changes in the STM contrast. Nevertheless, the simulated image in Fig. 4b is similar to the experimental images presented in Fig. 2a–ii. It is also worth noticing that the Cu(100) surface is known to form one-dimensional structures, as in the case of the oxygen induced reconstruction where 1 of every 4 rows in the <001> direction are missing [33]. Here we find that 2 out of every 5 rows are missing to provide more space for the 33° tilt of CO molecules, a consequence of CO-CO repulsion.

5. Conclusion

In summary, using HPSTM we showed that the Cu(100) surface breaks up into nanoclusters in the presence of CO gas. At pressures of 0.25 mbar the surface is decorated by small nanoclusters, e.g., square shaped 5 atom Cu nanoclusters stabilized by 4 CO molecules. As the CO pressure increases some of these nanoclusters merge into larger ones, while at the same time new structures in the form of 3-atom wide linear nanoclusters separated by two empty atomic rows form. These new structures can accommodate more CO molecules, while the repulsion between molecules causes them to tilt and to adopt a zigzag structure. DFT + U calculations provided the rationale behind nanoclusters formation as a result of the energy gained through CO adsorption on low coordinated Cu atoms, which provides the energy required to detach Cu atoms from step edges and form nanoclusters. Our work demonstrates that atomic scale studies of surfaces under gases in ambient conditions is crucial for a fundamental understanding of their role in catalysis and other chemical processes.

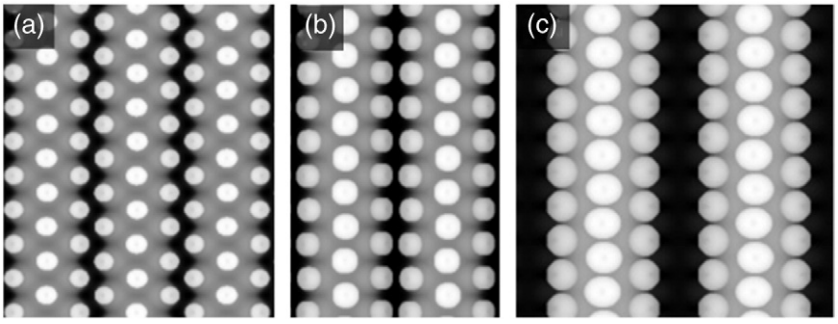

Fig. 4. Simulated STM images of the three atom wide linear clusters with periodicities of 4, 5 and 7 atoms from (a) to (c), respectively, obtained using the Hive graphic package [32]. The observed structure in Fig. 2b–ii matches best with the structure that exhibits periodicity every 5 atoms shown in (b).

Acknowledgments

This work was supported by the Office of Basic Energy Sciences (BES), Division of Materials Sciences and Engineering, of the U.S. Department of Energy (DOE) under contract no. DE-AC02-05CH11231, through the Chemical and Mechanical Properties of Surfaces, Interfaces (FWP KC3101). The calculations by D.Z. and L.-W.W. were supported by the "Organic/Inorganic Nanocomposite Materials" program. It used resources of the National Energy Research Scientific Computing Center which is supported by the Office of Science of the U.S. DOE. The computation also used the resources of Oak Ridge Leadership Computing Facility (OLCF) with the computational time allocated by the Innovative and Novel Computational Impact on Theory and Experiment (INCITE) project.

References

[1] G.A. Somorjai, Introduction to Surface Chemistry and Catalysis, Wiley-VCH, New York, 1999.
[2] G. Ertl, Angew. Chem. Int. Ed. 47 (2008) 3524.
[3] B.J. McIntyre, M. Salmeron, G.A. Somorjai, Rev. Sci. Instrum. 64 (1993) 687.
[4] L. Österlund, P.B. Rasmussen, P. Thostrup, E. Laegsgaard, I. Stensgaard, F. Besenbacher, Phys. Rev. Lett. 86 (2001) 460.
[5] E. Laegsgaard, L. Österlund, P. Thostrup, P.B. Rasmussen, I. Stensgaard, F. Besenbacher, Rev. Sci. Instrum. 72 (2001) 3537.
[6] F. Tao, D. Tang, M. Salmeron, G.A. Somorjai, Rev. Sci. Instrum. 79 (2008) 084101.
[7] F. Besenbacher, P. Thostrup, M. Salmeron, MRS Bull. 37 (2013) 677.
[8] C.T. Herbschleb, P.C. van der Tuijn, S.B. Roobol, V. Navarro, V.J.W. Bakker, Q. Liu, D. Stoltz, M.E. Cañas-Ventura, G. Verdoes, M.A. van Spronsen, M. Bergman, L. Crama, I. Taminiau, A. Ofitserov, G.J.C. van Baarle, J.W.M. Frenken, Rev. Sci. Instrum. 8 (2014) 083703.
[9] F. Tao, S. Dag, L.-W. Wang, Z. Liu, D.R. Butcher, H. Bluhm, M. Salmeron, G.A. Somorjai, Science 327 (2010) 850.
[10] B. Eren, D. Zherebetskyy, L.L. Patera, C.H. Wu, H. Bluhm, C. Africh, L.-W. Wang, G.A. Somorjai, M. Salmeron, Science 351 (2016) 475.
[11] K. Klier, Methanol synthesis, in: D.D. Eley, H. Pines, P.B. Weisz (Eds.), Advances in Catalysis, vol. 31, Academic Press, San Diego 1982, p. 243.
[12] D.S. Newsome, Catal. Rev. Sci. Eng. 21 (1980) 275.
[13] J. Szanyi, D.W. Goodman, Catal. Lett. 10 (1991) 383.
[14] J. Yoshihara, C.T.J. Campbell, J. Catal. 161 (1996) 776.
[15] M. Behrens, F. Studt, I. Kasatkin, S. Kühl, M. Hävecker, F. Abild-Pedersen, S. Zander, F. Girgsdies, P. Kurr, B.L. Kniep, M. Tovar, R.W. Fischer, J.K. Nørskov, R. Schlögl, Science 336 (2012) 893.
[16] G.A. Olah, Angew. Chem. Int. Ed. 52 (2013) 104.
[17] M. Behrens, Angew. Chem. Int. Ed. 53 (2014) 12022.
[18] H.-J. Freund, G. Meijer, M. Scheffler, R. Schlögl, M. Wolf, Angew. Chem. Int. Ed. 50 (2011) 10064.
[19] B. Eren, L. Lichtenstein, C.H. Wu, H. Bluhm, G.A. Somorjai, M. Salmeron, J. Phys. Chem. C 119 (2015) 14669.
[20] B. Eren, C. Heine, H. Bluhm, G.A. Somorjai, M. Salmeron, J. Am. Chem. Soc. 137 (2015) 11186.
[21] G. Kresse, J. Furthmuller, Phys. Rev. B 54 (1996) 11169.
[22] G. Kresse, D. Joubert, Phys. Rev. B 59 (1999) 1758.
[23] S.L. Dudarev, G.A. Botton, S.Y. Savrasov, C.J. Humphreys, A.P. Sutton, Phys. Rev. B 57 (1998) 1505.
[24] C.M. Truong, J.A. Rodriguez, D.W. Goodman, Surf. Sci. Lett. 271 (1992) L385.
[25] M. Dion, H. Rydberg, E. Schröder, D.C. Langreth, B.I. Lundqvist, Phys. Rev. Lett. 92 (2004) 246401.
[26] J. Ahner, D. Mocuta, R.D. Ramsier, J.T. Yates, J. Chem. Phys. 105 (1996) 6553.
[27] M. Poensgen, J.F. Wolf, J. Frohn, M. Giesen, H. Ibach, Surf. Sci. 274 (1992) 430.
[28] M.M. Waldrop, Science 234 (1986) 673.
[29] G. Román-Pérez, J.M. Soler, Phys. Rev. Lett. 103 (2009) 096102.
[30] P. Uvdal, P.-A. Karlsson, C. Nyberg, S. Andersson, Surf. Sci. 202 (1998) 167.
[31] J. Tersoff, D.R. Hamann, Phys. Rev. Lett. 50 (1983) 1998.
[32] D.E.P. Vanpoucke, G. Brocks, Phys. Rev. B 77 (2008) 241308(R).
[33] F.M. Leibsle, Surf. Sci. 337 (1995) 51.